

Facile Synthesis of Flower-like Ni(OH)₂/rGO Nanocomposite as Sensitive Electrochemical Sensor for Formaldehyde Detection

Shanjian Li*, Mao Li, Hao Yang, Jingyuan Shao, Zuchao Meng*

College of Chemistry and Chemical Engineering, Xi'an shiyou University, Xi'an Shaanxi 710065, China

*E-mail: 690920240@qq.com, zcmeng@xsyu.edu.cn

Received: 20 February 2022 / Accepted: 24 April 2022 / Published: 6 June 2022

Ni(OH)₂/rGO composite was synthesized facilly by using Ni-MOF/rGO composite as the precursor and derivatized by the solid-solid conversion in NaOH solution, which was green, simple and controllable. The morphology and structure of Ni(OH)₂/rGO composite was characterized by SEM and XRD. Due to the synergistic effect between flower-like Ni(OH)₂ and highly conductive rGO, a new kind of formaldehyde sensor with high electrocatalytic activity was prepared. The analytical performance of the formaldehyde sensor was investigated by Linear Scanning Voltammetry (LSV). The linear analysis range was 0.1 ~ 100 mM with the detection limit of 0.06 mM. In addition, the sensor is applied to the detection of formaldehyde in simulated water samples, and the recovery is between 97.9% and 110.4%.

Keywords: Ni(OH)₂, Graphene, Electrocatalysis, Formaldehyde, sensor

1. INTRODUCTION

Formaldehyde, a common environmental pollutant, is highly toxic. It has been identified by the U.S. EPA (U.S. Environmental Protection Agency) and the WHO (World Health Organization) as a harmful substance that causes deformity and cancer[1]. However, formaldehyde is widely used in daily foods, beverages, building materials, households, cosmetics and the organic chemical industry. Therefore, the establishment of an accurate and rapid method for the determination of trace formaldehyde has become a common research topic in recent years[2]. Among many methods for the determination of formaldehyde, the electrochemical method has been widely studied and applied because of its simple operation, high speed, and high sensitivity [3,4].

Because formaldehyde is not an electroactive organic compound, it is difficult to realize the electrocatalytic determination on the bare glassy carbon electrode. However, some studies have shown that the electrocatalytic oxidation of non-electroactive or high potential substances can be realized through the chemically modified electrode[5-10]. Metal organic framework materials (MOFs) are porous materials with large surface areas, diverse and variable structures and artificially controlled voids. They are widely used in the fields of gas storage, heterogeneous catalysis, fluorescence and others. They have open metal active sites, providing a theoretical basis for the preparation of electrochemical sensors[11]. Considering the poor stability of some MOFs materials, some researchers calcined MOFs in a nitrogen atmosphere to prepare porous carbon materials or carbon coated metal or metal oxide composites. And porous metal oxides are prepared by calcination in air or oxygen. These porous materials prepared by high temperature pyrolysis with MOFs as templates generally inherit some advantages of MOFs and surpass the corresponding traditional materials in many aspects such as morphology, specific surface area and porosity[12-14]. Therefore, electrochemical sensors based on these new porous materials have attracted strong attention of researchers[15]. Wei et al. [16] used HKUST-1 as a raw material to prepare ant mound-like Cu@C nanocomposites with a high surface area that showed good electrocatalytic performance for glucose. The constructed enzyme-free glucose electrochemical sensor had a wide linear range and a low detection limit. Ling et al.[17] first prepared porous carbon by pyrolysis of ZIF-8 in a nitrogen atmosphere, and then assembled it with porphyrin and glucose oxidase to prepare a novel glucose biosensor, which showed good accuracy in plasma sample analysis. When new porous materials are synthesized by a calcination method based on MOFs templates, there are high temperature and high pressure, high energy consumption and long synthesis time. In addition, the obtained metals or metal oxides are easy to agglomerate and lose their hierarchical structure in the process of thermolysis[18].

Therefore, it is necessary to develop a simple, easily controlled synthesis of porous metal oxides or metal hydroxides at normal temperature and pressure. In this work, porous Ni(OH)₂/rGO composite was prepared by solid-solid conversion in NaOH solution with Ni-MOF/rGO as template, and their electrocatalytic properties for formaldehyde were studied. This simple and controllable method of “large to small” synthesis of nano materials provides a research idea for the construction of a new formaldehyde electrochemical sensor based on porous nanomaterials.

2. EXPERIMENTAL

2.1 Apparatus and Reagents

A CHI660E electrochemical workstation (Chenhua Instruments Co., Ltd., Shanghai, China) was used for all the electrochemical experiments. A JSM-6700F scanning electron microscope (Japan Electronics Corporation, Japan) was applied to measure SEM and EDS images. A X'Pert PRO X-ray diffractometer (PANalytical, Almelo, the Netherlands) was implemented in XRD measurements.

Graphite powder (purity>99.85%, Sinopharm Chemical Reagent Co., Ltd), nickel nitrate(Tianjin Beilian Fine Chemicals Development Co., Ltd), terephthalic acid (Shanghai McLean Biochemical Technology Co., Ltd).

2.2 Preparation of Ni-MOF/rGO

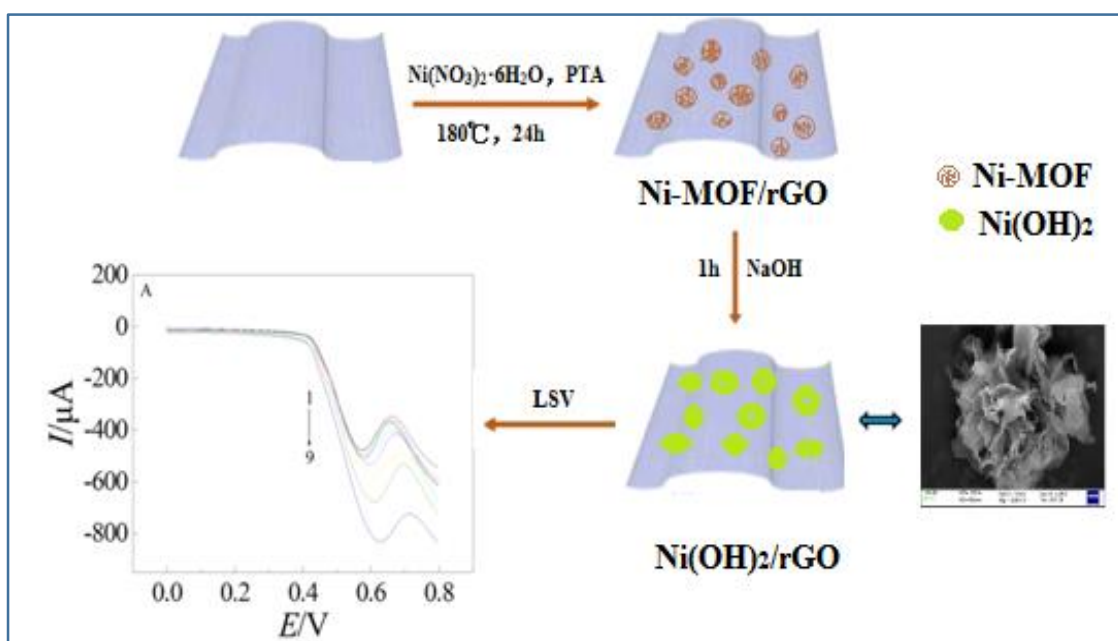
Reduced graphene oxide (rGO) was prepared by reducing graphene oxide with hydrazine hydrate[19]. Then 0.07 g rGO and 2.33 g $\text{Ni}(\text{NO}_3)_2 \cdot 6\text{H}_2\text{O}$ were added to 60 mL DMF, then 0.66 g PTA was added to them. After ultrasonic dispersion, the mixture is transferred to a stainless steel autoclave and reacted at 180 °C for 24 h. The obtained solid was dried at 60 °C for 24 h in a vacuum oven to obtain the Ni-MOF/rGO composite. Ni-MOF was prepared by the similar method without rGO.

2.3 Preparation of $\text{Ni}(\text{OH})_2/\text{rGO}$

0.16 g Ni-MOF/rGO and 20 mL 0.5 M NaOH were mixed uniformly, then they reacted at 60 °C for 1 h to obtain $\text{Ni}(\text{OH})_2/\text{rGO}$ composite.

2.4 Fabrication of $\text{Ni}(\text{OH})_2/\text{rGO}/\text{GCE}$

The bare glassy carbon electrode (GCE) was polished with $\alpha\text{-Al}_2\text{O}_3$, washed with ultrapure water, and then dried with N_2 for standby. 5 μL of 3 mg/mL $\text{Ni}(\text{OH})_2/\text{rGO}$ suspension was added on the surface of GCE, and then 0.05% Nafion was dropped on its surface to obtain $\text{Ni}(\text{OH})_2/\text{rGO}/\text{GCE}$. For comparison, rGO/GCE, Ni-MOF/GCE can be fabricated similarly. The electrochemical detection of formaldehyde can be realized by using $\text{Ni}(\text{OH})_2/\text{rGO}/\text{GCE}$ in 0.1 M KOH. The overall process has been shown in Scheme 1.



Scheme 1. The synthesis of $\text{Ni}(\text{OH})_2/\text{rGO}$ composite and the detection of formaldehyde on the $\text{Ni}(\text{OH})_2/\text{rGO}/\text{GCE}$

3. RESULTS AND DISCUSSION

3.1 SEM and mapping analysis

The SEM images of Ni-MOF/rGO and Ni(OH)₂/rGO composites were showed in Fig. 1. It can be seen that both Ni-MOF/rGO and Ni(OH)₂/rGO were both flower-like, but compared with Ni-MOF/rGO composite, Ni(OH)₂/rGO composite, which had larger petals, was looser, leading to its higher surface area and improved electrocatalytic performance. In the mapping analysis (Fig. 1c-e), the presence of C, O and Ni can be seen, which further confirmed that Ni(OH)₂/rGO composite has been successfully prepared.

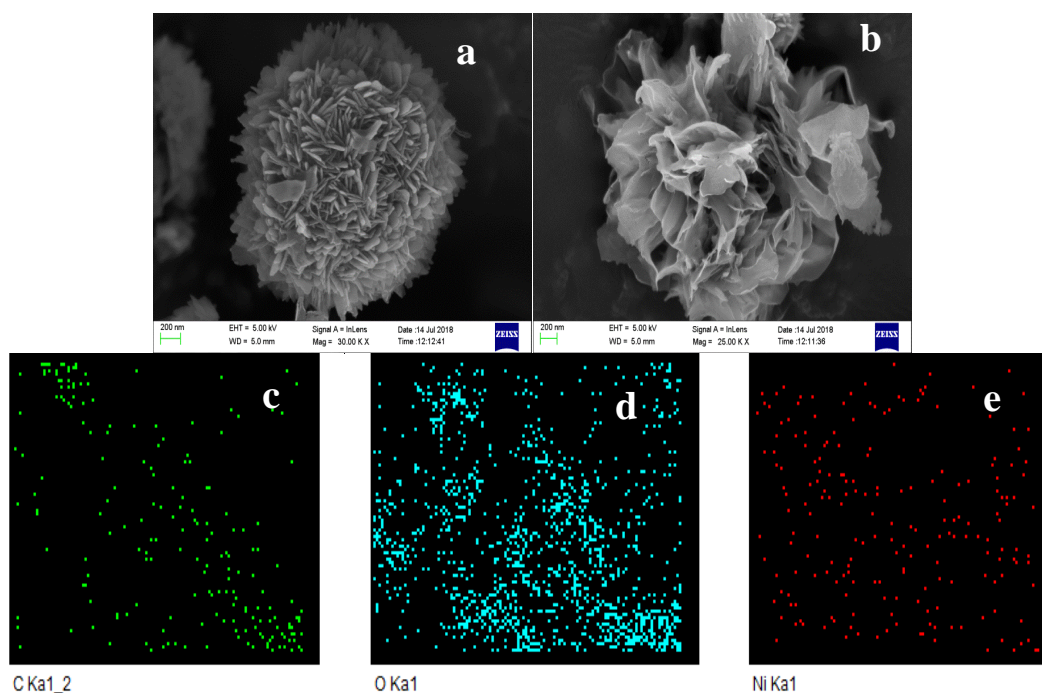


Figure 1. SEM images of Ni-MOF/rGO (a) and Ni(OH)₂/rGO (b) mapping analysis of C (c), O(d) and Ni(e)

3.2 XRD analysis of Ni(OH)₂/rGO Composite

Fig. 2 is the XRD spectrum of Ni(OH)₂/rGO composite, in which the characteristic diffraction peaks at 19.92°, 33.11°, 44.43°, 51.75° and 59.08° are consistent with the diffraction peaks of (001), (100), (101), (102) and (110) crystal planes of β -Ni(OH)₂[20], indicating that Ni(OH)₂ has been successfully prepared. However, the characteristic diffraction peaks of rGO is not seen in the spectrum possibly due to the low rGO content.

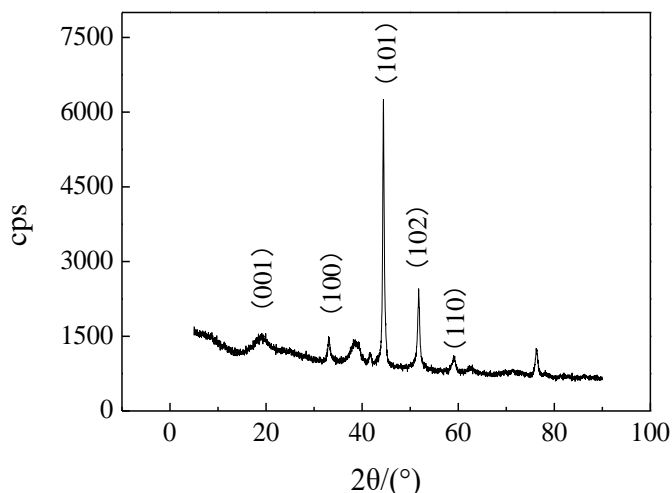


Figure 2. XRD pattern of Ni(OH)₂/rGO composite

3.3 Calculation of the effective surface area of different electrodes

0.1 mM K₃[Fe(CN)₆] used as a probe, and the effective electrode areas of different electrodes were calculated by chronocoulometry.

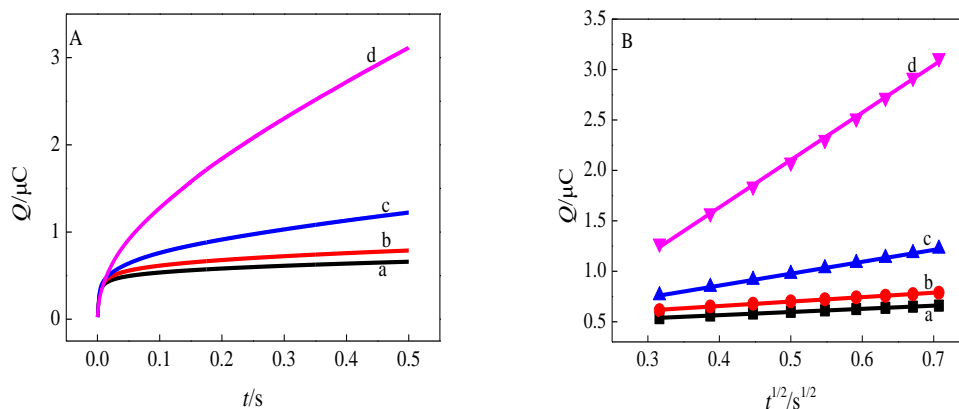


Figure 3. (A) $Q-t$ curve of rGO/GCE(a), Ni-MOF/GCE(b), Ni-MOF/rGO/GCE(c), Ni(OH)₂/rGO/GCE(d). (B) The plot of $Q-t^{1/2}$

The experimental results were shown in Fig. 3. The linear curve of $Q-t^{1/2}$ can be obtained from the $Q-t$ curve (Fig. 3B), and then the effective surface area of different modified electrode can be calculated according to the Anson equation (Eq. 1) and the slope of $Q-t^{1/2}$ curve relationship. The effective electrode areas of rGO/GCE, Ni-MOF/GCE, Ni-MOF/rGO/GCE and Ni(OH)₂/rGO/GCE were 0.17 cm², 0.24 cm², 0.33 cm² and 0.52 cm², respectively. The effective surface area of Ni(OH)₂/rGO/GCE is the largest due to the unique flower-like structure of Ni(OH)₂/rGO composite.

$$Q(t) = \frac{2nFAcD^{1/2}t^{1/2}}{\pi^{1/2}} + Q_{dl} + Q_{ads} \quad (1)$$

where n is the number of transferred electrons, A the effective surface area of electrode (cm^2), C the concentration of active substance (mol/cm^3), D the diffusion coefficient ($D=7.6 \times 10^{-6} \text{ cm}^2 \cdot \text{s}^{-1}$), Q_{dl} the double layer charge, which can be eliminated by subtracting the background charge, Q_{ads} the Faraday power, F the faraday constant.

3.4 Electrochemical behavior of formaldehyde on the Ni(OH)₂/rGO/GCE

CVs of formaldehyde on the different electrodes were showed in Fig. 4. It can be seen that Ni(OH)₂/rGO composite showed the highest electrocatalytical performance, compared to the others, which was mainly due to the high specific surface area of Ni(OH)₂/rGO composite and the good synergistic properties between Ni(OH)₂ and rGO.

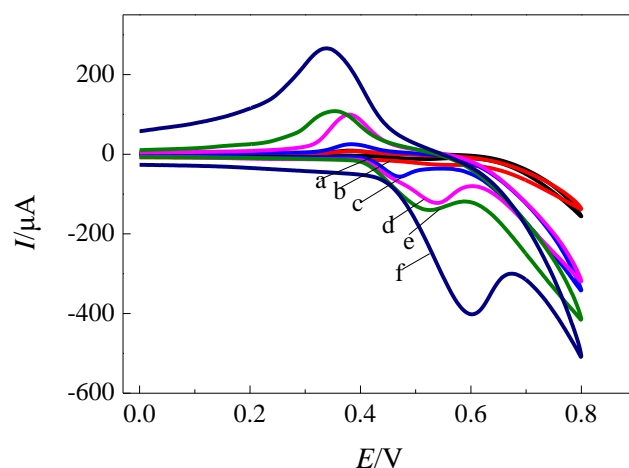
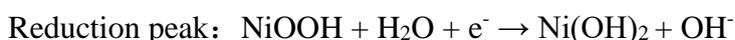
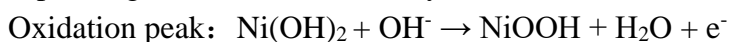


Figure 4. The CV curves on the GCE (a), rGO/GCE (b), Ni-MOF/GCE (c), Ni-MOF/rGO/GCE (d), Ni(OH)₂/rGO/GCE (f) in 0.1 M KOH containing 1 mM formaldehyde and Ni(OH)₂/rGO/GCE in 0.1 M KOH without formaldehyde (e)

In order to further verify the electrocatalytic performance of Ni(OH)₂/rGO composite for formaldehyde, the CVs of formaldehyde with different concentrations were measured at the scanning rate of $0.1 \text{ V} \cdot \text{s}^{-1}$ in 0.1 M KOH. The experimental results were shown in Fig. 5. Fig. 5 showed that a pair of redox peaks appeared in 0.1 M KOH without formaldehyde, and according to the literature [21], the corresponding electrode reaction may be as follows.



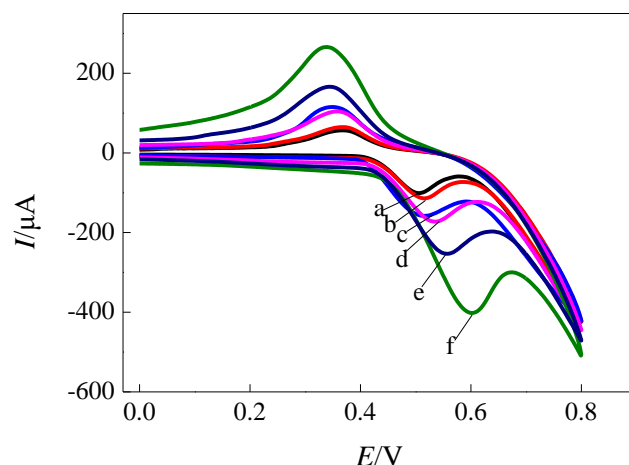


Figure 5. CV Curves of formaldehyde of different concentrations on the Ni(OH)₂/rGO/GCE (a~f: 0, 0.25, 0.50, 0.75, 1.00, 1.25 mM)

Fig. 5 also showed that with the increasing formaldehyde concentrations, the peak currents of oxidation peak and reduction peak gradually increase, indicating that Ni(OH)₂/rGO composite had obvious electrocatalytic performance for formaldehyde.

3.5 Effect of the scan rate

The cyclic voltammetric behaviors of formaldehyde on the Ni(OH)₂/rGO/GCE at different scanning rates were shown in Fig. 6A. With the increase of scanning rate, I_{pa} also increases. At the same time, it can be seen in Fig. 6B, I_{pa} has a linear relationship with the square root of scanning rate ($v^{1/2}$) in the range of 10~120 $\text{mV}\cdot\text{s}^{-1}$, and the corresponding linear equation is $I_{pa}=1.40-1148.50 v^{1/2}$ ($R=0.9995$). It shows that the electrocatalytic process of formaldehyde on the Ni(OH)₂/rGO/GCE is mainly controlled by the diffusion process. In addition, the oxidation peak potentials (E_{pa}) gradually shifted positively with the increase of scan rate in Fig. 6(A). The linear equation between E_{pa} and the logarithm of scanning rate was $E_{pa}=0.68047+0.081 \log v$ ($R=0.9929$) (Fig. 6C). According to Laviron (Eq.2)[22], Bard and Faulkner (Eq.3)[23], and the linear slope of $E_{pa}-\log v$ curve, the number of electrons transferred n for the electrocatalytic oxidation of formaldehyde on the Ni(OH)₂/rGO/GCE was calculated to be 2.

$$E_p = E^0 + \left(\frac{2.303RT}{\alpha nF}\right) \log\left(\frac{RTk^0}{\alpha nF}\right) + \left(\frac{2.303RT}{\alpha nF}\right) \log v \quad (2)$$

$$\alpha = \frac{47.7}{(E_p - E_{p/2}) \text{mV}} \quad (3)$$

In the above equations, α is the transfer coefficient, k^0 the standard rate constant, n the number of transferred electrons, v the scan rate and E^0 is the formal redox potential. $E_{p/2}$ the potential where the current is half of the peak current. Other symbols get their usual meanings.

Therefore, the possible reaction equation of formaldehyde is as follows.



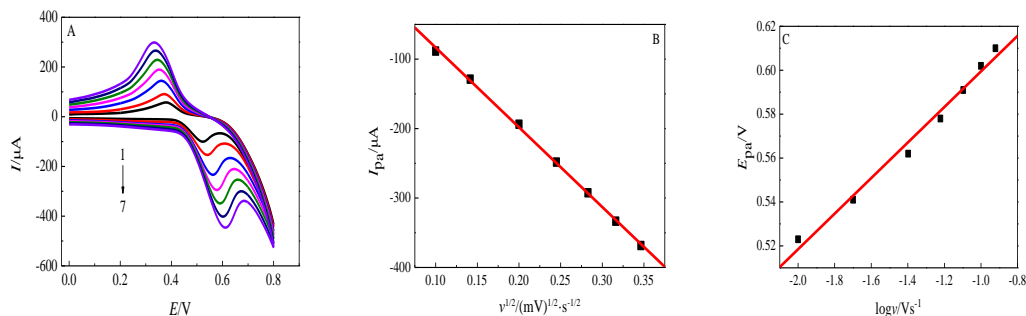


Figure 6. (A) CVs of 1mM formaldehyde on the Ni(OH)₂/rGO/GCE in 0.1 M KOH at different scan rates (from 1-7): 0.01, 0.02, 0.04, 0.06, 0.08, 0.1, 0.12 V·s⁻¹. (B) The plot between I_{pa} and $v^{1/2}$. (C) The plot between E_{pa} and $\log v$.

3.6 Effect of quiet time

To optimize the experimental conditions for the detection of formaldehyde, the quiet time was studied. The CV Curves of formaldehyde at different quiet time on the Ni(OH)₂/rGO/GCE were shown in Fig. 7A. In Fig. 7B, it can be seen that when the quiet time was less than 12s, I_{pa} increased significantly with the increase of quiet time, while when the quiet time is more than 12s, I_{pa} exhibited no obvious change with the increase of quiet time. The results showed that the adsorption of formaldehyde reached saturation on the Ni(OH)₂/rGO/GCE. Therefore, the quiet time selected in this experiment was 12s.

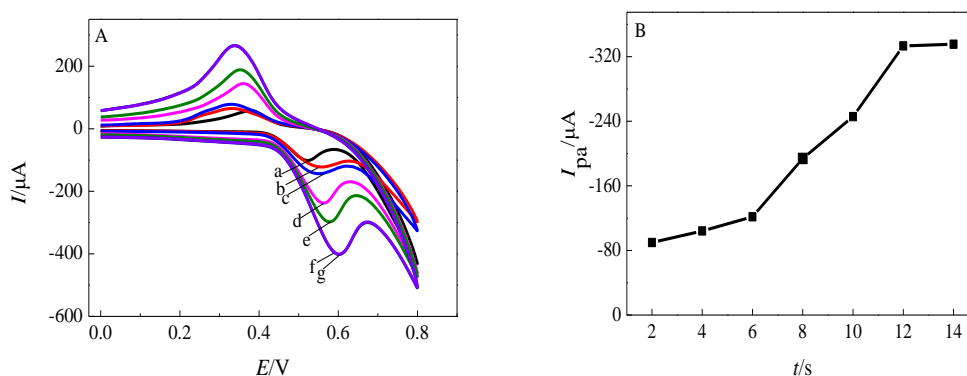


Figure 7. (A) The CV Curves of 1 mM formaldehyde at different quiet time on the Ni(OH)₂/rGO/GCE (a-g : 2, 4, 6, 8, 10, 12, 14s). (B) The plot between I_{pa} and quiet time.

3.7 Detection of formaldehyde

The results for the detection of formaldehyde by LSV were shown in Fig. 8. The linear relationship between I_{pa} and formaldehyde concentration was in the range of 0.1-100 mM (Fig. 8b). And the linear relationship was $I_{pa}(\mu A) = -444.70 - 24.72 C$ ($R = -0.9971$) with the detection limit of 0.06 mM ($S/N=3$).

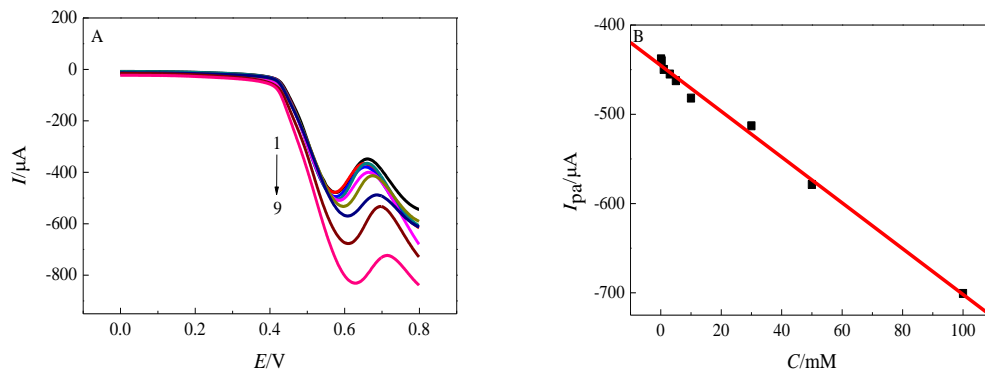


Figure 8. (a) Linear sweep voltammograms of formaldehyde with different concentrations on the Ni(OH)₂/rGO/GCE (1-9 : 0.1, 0.3, 1, 3, 5, 10, 30, 50, 100 mM). (b) The relationship between formaldehyde concentration and I_{pa} .

The comparisons between some efficient formaldehyde sensors were presented in Table 1. Seen from Table 1, the formaldehyde electrochemical sensor based on the Ni(OH)₂/rGO/GCE has a wider linear range than the previous reports[23-28].

Table 1. Comparison of different chemical modified electrodes for the determination of formaldehyde

Electrode	Linear range	Detection limit/ μ M	Reference
CuO/Cu/TiO ₂	65.0 μ M - 7.80 mM	25.0	24
Pt-Pd/GCE	10 μ M - 1 mM	3	25
Pd nanowire /GCE	2 μ M - 1 mM	0.5	26
Fe@Pt/C	12.5 μ M - 15.4 mM	--	27
Pd-Cu-SBA-16/CPE	1.79 mM - 121.86 mM	16	28
AgPd/Ch-IL/GCE	0.060mM- 20mM	22	29
Ni(OH) ₂ /rGO/GCE	0.1mM - 100 mM	60	This work

3.8 Interference, reproducibility and stability

The stability and reproducibility of the formaldehyde electrochemical sensor based on the Ni(OH)₂/rGO/GCE were evaluated. Using the same Ni(OH)₂/rGO/GCE for 10 consecutive parallel experiments in 1mM formaldehyde, the RSD of I_{pa} is 3.8%, which proves that the formaldehyde electrochemical sensor based on the Ni(OH)₂/rGO/GCE has good stability and can be used for repeated detection of formaldehyde. At the same time, six formaldehyde electrochemical sensors based on the Ni(OH)₂/rGO/GCE were prepared. Their electrocatalytic properties for 1 mM formaldehyde were studied respectively. The RSD of I_{pa} was 3.2%, indicating that the formaldehyde electrochemical sensors have good reproducibility. In addition, in order to investigate the anti-interference of the formaldehyde

electrochemical sensors, 100 times of anions and cations such as K^+ , Na^+ , Cl^- , NO_3^- and SO_4^{2-} , 100 times of phenol, benzene and acetone, and 5 times of methanol, ethanol and glycerol were added to the 0.1 M KOH solution containing 1 mM formaldehyde. The results showed that the determination error of formaldehyde content was less than 5%, indicating the sensor had strong anti-interference capacity.

3.9 Analytical application in real samples

The formaldehyde sensor based on $Ni(OH)_2/rGO/GCE$ was used to detect formaldehyde in real samples. Three simulated wastewater samples containing 100 μM formaldehyde were analyzed. It can be seen in Table 2 that the recovery of formaldehyde was 97.9%~110.4%, indicating that the formaldehyde sensor based on $Ni(OH)_2/rGO/GCE$ could be used effectively for the determination of formaldehyde in real samples.

Table 2. Detection results of formaldehyde based on $Ni(OH)_2/rGO/GCE$

Sample	Formaldehyde content / μM	Formaldehyde added / μM	Formaldehyde found / μM	Recovery/%
1	100	50	155.2	110.4
2	100	100	198.6	98.6
3	100	150	246.8	97.4

4. CONCLUSIONS

Under normal temperature and pressure, the Ni-MOF/rGO composite used as a precursors, flower-like $Ni(OH)_2/rGO$ composite were obtained by solid-solid conversion in NaOH solution. The process was green, simple and easy to control. A new formaldehyde electrochemical sensor based on $Ni(OH)_2/rGO/GCE$ is fabricated. The formaldehyde electrochemical sensor has good electrocatalytic activity for formaldehyde with a wide linear range and a low detection limit, which is due to the larger surface area and good conductivity of the $Ni(OH)_2/rGO$ composite, which improved the electron transfer efficiency between the modified electrode and the formaldehyde.

ACKNOWLEDGMENTS

This work was financially supported by Shaanxi Provincial Natural Science Foundation (No. 2018JM2014), Industrial research project of Science and Technology Department of Shaanxi Province (No. 2022GY-144).

COMPLIANCE WITH ETHICAL STANDARDS

The author(s) declare that they have no competing interests.

References

1. S. Huang, W. Wei, W. B. Louise, S. Tunga, H. Kan, Z. Bu and Y. Zhang, *Sci. Total. Environ.*, 590 (2017) 394.
2. M. Guglielmino, A. Allouch, C.S. Le and C.A. Serra, *Sensor. Actuat. B-Chem.*, 243 (2016) 963.
3. M. Guglielmino, P. Bernhardt, C. Trocquet, C.A. Serra and S.L. Calvé, *Talanta*, 172 (2017) 102.
4. J.H. He, S.T. Zhang, Y.H. Cai and Z.R. Song, *Asian J. Chem.*, 25 (2013) 10121.
5. B. Dinesh, R. Saraswathi and A.S. Kumar, *Electrochim. Acta*, 233 (2017) 92.
6. S.N. Azizi, S. Ghasemi and F. Amiripour, *Sensor. Actuat. B-Chem.*, 227 (2016) 1.
7. S.L. Zhang, X. Wen, J.J. Xia, J.Q. Hu and A.D. Tang, *J. Alloys. Compd.*, 829 (2020) 154568.
8. H. Mei, W. Wu, B. Yu, H. Wu, S. Wang and Q. Xia, *Sensor. Actuat. B-Chem.*, 223 (2016) 68.
9. X. Tang, N. Mager, B. Vanhorenbeke, S. Hermans and J.P. Raskin., *Nanotechnology*, 28 (2016) 055501.
10. O.K. Farha, A.M. Shultz, A.A. Sarjeant, S.B.T. Nguyen and J.T. Hupp, *J. Am. Chem. Soc.*, 133 (2011) 5652.
11. H. Hosseini, H. Ahmar, A. Dehghani, A. Bagheri and A. Tadjarodi, *Biosens. Bioelectron.*, 42 (2013) 426.
12. H. Hosseini, H. Ahmar, A. Dehghani, A. Bagheri, A.R. Fakhari and M.M. Amini, *Electrochim. Acta.*, 88 (2013) 301.
13. S. Wang, Y. Hou, S. Lin and X.C. Wang, *Nanoscale*, 6 (2014) 9930.
14. W. Zhang, X.F. Jiang, Y.Y. Zhao, Arnau.Carné-Sánchez, Victor.Malgras, Jeonghun.Kim, Jung.Ho, S.B. Wang, J. Liu, Ji-Sen, Yusuke. Yamauchi and M. Hu, *Chem. Sci.*, 8 (2017) 3538.
15. Y. Song, C. Wei, J. He, L. Xia, X. Lu and W. Li, *Sensor. Actuat. B-Chem.*, 220 (2015) 1056.
16. C. Wei, X. Li, F. Xu, H. Tan, Z. Li, L. Sun and Y. Song, *Anal. Methods*, 6 (2014) 1550.
17. P.H. Ling, Q. Hao, J.P. Lei and H.X. Ju, *J. Mater. Chem. B*, 3 (2015) 1335.
18. B. Liu, X. Zhang, H. Shioyama, T. Mukai, T. Sakai and X. Qiang, *J. Power Sources*, 195 (2010) 857.
19. C.R. Minitha, V.S. Anithaa, V. Subramaniam and R.T.R. Kumar, *A.C.S. Omega*, 3 (2018) 4105.
20. X. Wen, J. Xi, M. Long, L. Tan, J. Wang, P. Yan, L. Zhong, Y. Liu and A. Tang, *J. Electroanal. Chem.*, 6657 (2017) 30702.
21. W. Xing, S. Qiao, X. Wu, X. Gao, J. Zhou, S. Zhuo, S.B. Hartono and D. Hulicova-Jurcakova, *J. Power Sources*, 196 (2011) 4123.
22. E. Laviron, *J. Electroanal. Chem.*, 101 (1979) 19.
23. A.J. Bard, L.R. Faulkner, *Electrochemical Methods Fundamentals and Application*, Wiley (2004) New York, USA.
24. S. Zhang, X. Wen, M. Long, J. Xi, J. Hu and A. Tang, *J. Alloys Compd.*, 829 (2020) 154568.
25. Z.L. Zhou, T.F. Kang, Y. Zhang and S.Y. Cheng, *Microchim. Acta*, 164(2009)133.
26. Y. Zhang, Z. Min, Z. Cai, M. Chen and F. Cheng, *Electrochim. Acta*, 2012, 68 (319)172.
27. M. He, W.Q. Wu, B.B. Yu, H.M. Wu, S.F. Wang and Q.H. Xia, *Sensor. Actuat. B-Chem.*, 223 (2016) 68.
28. S. Kaviani, S.N. Azizi and S. Ghasemi, *J. Electroanal. Chem.*, 799 (2017) 308.
29. M.R. Mahmoudian, W.J. Basirun, P.M. Woi, H. Hazarkhani and Y. B. Alias, *Microchim. Acta*, 369(2019)186.